RSC Advances

ROYAL SOCIETY OF CHEMISTRY

www.rsc.org/advances

RSC Advances

ARTICLE

Facile fabrication of thermally reduced graphene oxide-platinum nanohybrids and their application in catalytic reduction and dye-sensitized solar cells

Received 00th January 20xx,
Accepted 00th January 20xx

DOI: 10.1039/x0xx00000x

www.rsc.org/

Nguyen Tri Khoa,[a,c] Doan Van Thuan,[a,c] Soon Wook Kim,[a] Sujung Park,[a] Tran Van Tam,[b] Won Mook Choi,[b] Shinuk Cho,[a] Eui Jung Kim,[b*] and Sung Hong Hahn[a*]

We report the fast synthesis of thermally reduced graphene oxide: platinum (TRGO:Pt) nanohybrids by simply spraying GO:Pt^{4+} solution on a hot plate. X-ray photoelectron spectroscopy and atomic force microscopy analyses are performed to investigate the thermal reduction of GO:Pt^{4+} and the morphologies of TRGO:Pt hybrid monolayer, respectively. The catalytic performance of TRGO:Pt is evaluated for the reduction of o-nitroaniline. A significant increase in the reaction rate constant for TRGO:Pt compared with pure Pt is due to facilitated electron transfer at TRGO:Pt interface and enhanced catalytic active sites. Effective electron transfer from TRGO to Pt and significantly increased catalytic active sites in hybrids suggest that TRGO:Pt is a highly potential counter electrode material in dye-sensitized solar cells (DSSCs). The hybrid provides numerous electrons to Γ/I_3^- electrolyte to reduce the recombination at interface. As a result, the performance of DSSCs with TRGO:Pt hybrid electrode is significantly increased 34% in comparison with pure Pt electrode.

Introduction

Numerous efforts have been recently made to improve the efficiency of dye-sensitized solar cells (DSSCs), which are promising photovoltaic devices, and to reduce their manufacturing costs[1-7]. Typically, the operational principles of DSSCs are based on the generation and diffusion of electrons at interfaces such as injection of photoinduced electrons from dye, diffusion of electrons through semiconductor, and regeneration of oxidized dye (receiving electrons from electrolyte) and reduced electrolyte at counter electrode interface (charge transfer reaction through catalytic activity at counter electrode)[8-11]. The interfacial structure of TiO_2/ruthenium-based dye/iodide-triiodide redox couple electrolyte/platinum (Pt) counter electrode has been mostly used in the fabrication of high-performance DSSCs[12-15]. Especially, catalytic reduction at the counter electrode surface is crucial in producing surplus electrons that are transferred to the electrolyte to regenerate oxidized dye, which greatly affects the conversion efficiency of DSSCs. Several materials have been employed in the fabrication of the counter electrode of DSSCs such as a thin catalytic Pt layer on conducting glass substrate[16,17], carbon material (carbon black, graphene, carbon nanotube)[18-20], and graphene-based composite material[21-25]. Graphene-based composites have recently attracted attention in fabricating low-cost and high-performance counter electrode of DSSCs due to its large specific surface area, excellent catalytic activity support, and high conductivity of graphene[26-31]. Ahn et al. reported a superior performance of p-doped 3D graphene/Pt hybrid as the counter electrode of a DSSC.[26] The DSSC efficiency of graphene-based hybrid counter electrode (8.46%) was 6% greater than that of Pt counter electrode (7.98%). Lin et al. developed nitrogen-doped graphene/platinum hybrid for use as the counter electrode to enhance the DSSCs efficiency.[27] The hybrid electrode showed the best performance of 9.38% which increased by 25% in comparison with the Pt counter electrode (7.53%).

In this article, we synthesize thermally reduced graphene oxide (TRGO):Pt hybrid using a novel and simple spray pyrolysis method and test the hybrid as the counter electrode of DSSCs. X-ray photoelectron spectroscopy (XPS) and atomic force microscopy (AFM) are used to study the bond interactions and surface morphologies of the hybrid. The synthesized TRGO:Pt hybrid exhibits enhanced catalytic performance and high durability for catalytic hydrogenation. The TRGO:Pt hybrid provides surplus electrons to reduce a redox couple in the electrolyte resulting in a significant increase the efficiency of DSSCs to 5.74% (34% increase) compared with the Pt counter electrode (4.31%). We demonstrate that the TRGO:Pt hybrid is a promising counter electrode material of DSSCs.

Experimental

Preparation of TRGO:Pt hybrid

[a] Department of Physics and Energy Harvest-storage Research Center, University of Ulsan, Ulsan 680-749, South Korea. *Email: shhahn@ulsan.ac.kr; Tel: +82-52-259-2330.
[b] Department of Chemical Engineering, University of Ulsan, Ulsan 680-749, South Korea. #Email: ejkim@ulsan.ac.kr; Tel: +82-52-259-2832.
[c] These authors contributed equally to this work.

0.1 mL of 8 %wt H_2PtCl_6 in H_2O (Sigma Aldrich) was diluted in 5 mL of ethanol. 1, 3, 5, and 7 mL of colloidal GO (0.3 g/L) synthesized using a modified Hummers method were added to the diluted solution, which was followed by stirring for 30 min. The final solution was sprayed on FTO substrate (for DSSCs study) and quartz substrate (for catalytic measurement) on a hot plate at 150 ^oC. The sprayed sample was burned on the hot plate at 350 ^oC for 20 min to thermally reduce graphene oxide to TRGO and Pt^{4+} to Pt and to improve the adhesion of the thin film coated on the substrate.

Fabrication of DSSCs

A TiO_2 paste (Ti-Nanoxide T/SP, Solaronix) was coated on FTO substrate using a doctor-blade technique and was then annealed at 500 ^oC for 60 min in air. To adsorb a sensitizing dye, the annealed mesoporous TiO_2 film was immersed in 0.3 mM Z907 dye solution ($C_{42}H_{52}N_6O_4RuS_2$, Sigma-Aldrich) in a mixture of acetonitrile: tert-butyl alcohol (1:1 v/v) at room temperature for 6 h. DSSCs were assembled onto two substrates of photoanode and counter electrode using a thermoplastic foil. The iodide/tri-iodide electrolyte (I^-/I_3^-, Iodolyte AN-50, Solaronix) was injected into the space between the photoanode and photocathode through a hole in the counter electrode substrate.

Catalytic hydrogenation measurement

The catalytic hydrogenation performance of TRGO:Pt hybrids was evaluated for the reduction of o-nitroaniline to 1,2-benzenediamine. Sodium borohydride ($NaBH_4$) was used as a hydrogen source for hydrogenation reaction. A mixture of 3 mL of 0.75 mM o-nitroaniline and 2 mL of 0.22 M $NaBH_4$ was stirred in 17 mL of deionized water for 5 min. The prepared TRGO:Pt on quartz substrate was placed in the o-nitroaniline solution to initiate the reduction reaction. UV-vis spectroscopy (HP8453) was employed to monitor the concentration of o-nitroaniline by measuring the absorption intensity at 410 nm.

Photo-conversion efficiency measurement

The photo-conversion efficiency of the DSSCs was evaluated using a PEC-L11 model 13 (Pecell Technologies Inc.) under simulated AM 1.5 illumination at an intensity of 100 mW/cm^2. The intensity of sunlight illumination was calibrated using a standard Si-photodiode detector with a KG-5 filter.

Characterization

Chemical bonding was investigated using a X-ray photoelectron spectroscopy (Thermal Fisher, K-alpha, XPS) and a FT-IR spectrometer (Varian 670/620). The surface morphologies of the samples were examined using field emission scanning electron microscopy (SEM, JEOL, JSM6500F) with a 10 kV operating voltage, atomic force microscopy (AFM, Veeco, Multimode V) with RTESP probe in a tapping mode, and transmission electron microscopy (TEM, JOEL, JEM-2200FS) with a 200 keV electron gun. The cyclic voltammetry with three electrodes including the Pt counter electrode, the Ag/AgCl reference electrode, and the working electrode (TRGO, Pt and TRGO:Pt) was performed using an electrochemical workstation (CHI 660E) in a solution of I^-/I_3^- and 0.1 M LiCl in ethanol at a scan rate of 50 mV/s. The electrochemical impedance of the samples was measured using an impedance spectroscopy (IviumStat, Ivium Tech) in the frequency range of 1-10^6 Hz.

Results and discussion

Figure 1 shows the XPS spectra of GO:Pt^{4+} (before thermal treatment) and TRGO:Pt (after thermal treatment at 350 ^oC for 20 min). The Pt4f surveys (Fig. 1a, c) reveal the presence of Pt(0), Pt(II), and Pt(IV) and the C1s scans (Fig. 1b, d) show the presence of C-C and other carbon groups in graphene network. As shown in Fig. 1a, the bonding energies of metallic Pt(0) are 72.1 eV ($Pt4f_{7/2}$) and 75.4 eV ($Pt4f_{5/2}$)[32]. Ionic Pt(II) and Pt (IV) peaks appear at 73.0 and 74.4 eV for $Pt4f_{7/2}$; 76.8 eV and 77.9 eV for $Pt4f_{5/2}$, respectively[32]. After thermal treatment, the binding energy of Pt decreases and the metallic Pt(0) peak intensity significantly increases. The ratios of Pt(0):Pt(II) and Pt(0):Pt(IV) in $Pt4f_{7/2}$ binding peak intensity are significantly increased from 0.46 and 0.18 (before annealing) to 2.45 and 3.06 (after annealing), respectively. These results indicate the formation of metallic Pt in the composite.

The thermal treatment of GO reduces the intensity of peaks related to oxygen functional groups as shown in Fig. 1b, d. The C-C binding energy slightly increases from 284.3 to 284.5 eV after thermal reduction process. Hydroxyl (C-OH), carbonyl (C=O), and carboxylate (HO-C=O) groups have their binding energies at 286.3, 287.8, 289.0 eV, respectively[33]. The oxygen functional groups in graphene network such as C-OH, C=O, and HO-C=O are greatly reduced after thermal reduction process. The C-OH, C=O, and O-C=O to C-C peak intensity ratio is decreased from 0.71, 0.20, and 0.15 to 0.13, 0.09, and 0.06 after annealing, respectively. Thus, by simply placing the sample on a hot plate at 350 ^oC for 20 min, GO and Pt^{4+} are easily reduced to TRGO and metallic Pt, respectively. The FT-IR spectra of GO and TRGO are shown in Figure S1 indicating that the oxygen-related functional groups of GO are greatly reduced after thermal reduction.

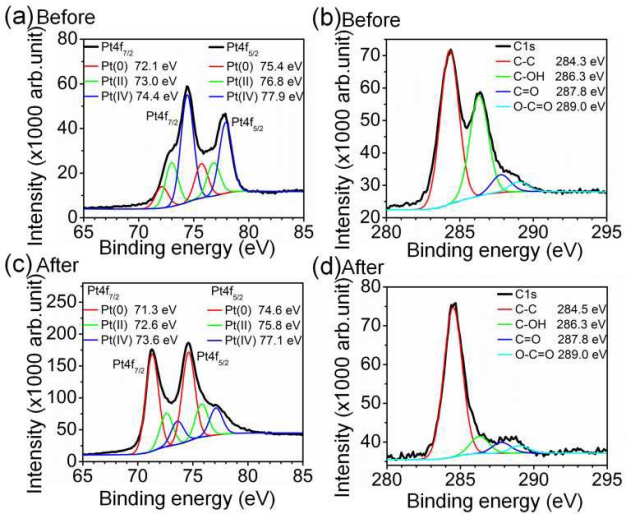

Figure 1: XPS spectra of TRGO:Pt before (a, b) and after (c, d) thermal treatment.

The AFM images of the samples are shown in Fig. 2. After thermal treatment of the as-sprayed H_2PtCl_6 solution, a smooth Pt film is formed on the substrate (Fig. 2a). One can see that the Pt film consists of Pt nanoparticles that are produced from the thermal reduction of Pt^{4+} precursor. Some Pt clusters are observed that result from the aggregation of nanoparticles. The surface roughness of the TRGO:Pt film is higher than that of the Pt film (Fig. 2b). The AFM image of Pt-decorated TRGO monolayer is illustrated in Fig. 2c. The thickness of the TRGO monolayer is found to be about 1.78 nm and Pt nanoparticles decorated onto the TRGO monolayer are 3-15 nm in size. In the absence of GO, spraying H_2PtCl_6 colloidal on the substrate results in a smooth Pt film which consists of aggregated Pt^{4+} particles. In the TRGO:Pt hybrid, GO serves as a stabilizer that adsorbs Pt^{4+} particles onto its negative network[34], thus preventing the aggregation of Pt particles and forming nanoparticle structure during thermal reduction process. Because of the excellent adsorption ability and hydrophilic properties of colloidal GO, Pt^{4+} is easily adsorbed onto the surface of GO nanosheets. After thermal reduction, Pt nanoparticles formed are evenly distributed over TRGO nanosheets as shown in Fig. 2c.

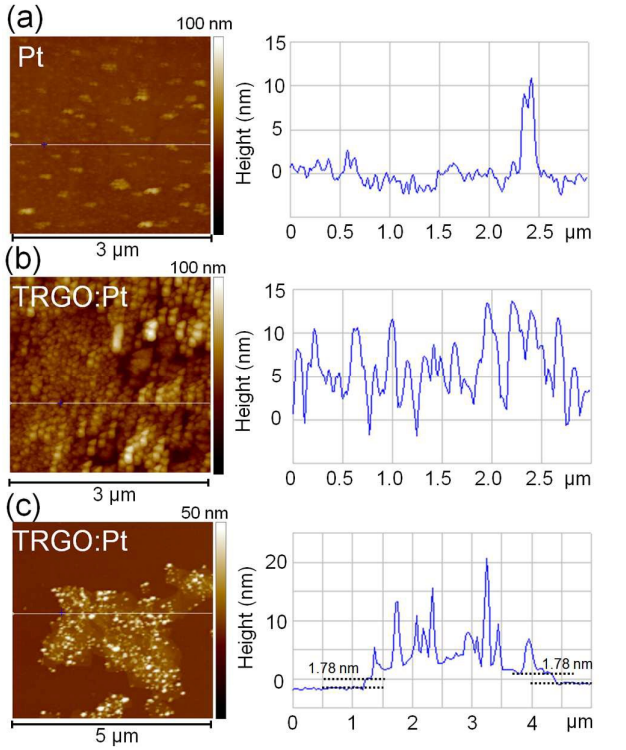

Figure 2. AFM images of pure Pt thin film (a), TRGO:Pt thin film (b) and TRGO:Pt monolayer (c).

Figure 3 shows the TEM images of TRGO:Pt hybrid catalyst. As shown in Fig. 3, the size of Pt nanoparticles is 3-15 nm, which is consistent with the AFM results. One can see that the Pt nanoparticles are evenly distributed over TRGO nanosheets. High resolution TEM image and corresponding FFT pattern in Fig. S2 indicate the formation of crystalline TRGO:Pt hybrids. The (111) and (200) diffraction spots of Pt nanoparticles and (002) spot of graphene are clearly observed in the FFT pattern.

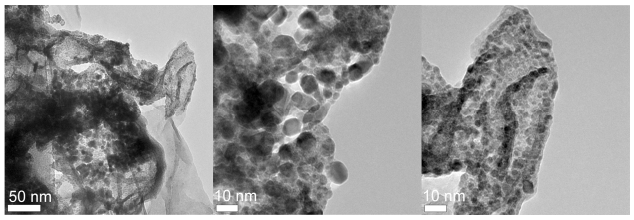

Figure 3. TEM images of TRGO:Pt hybrid catalyst.

The catalytic reduction efficiency of o-nitroaniline into 1,2-benzenediamine is shown in Fig. 4. The ratio in the TRGO-Pt nanohybrid sample name refers to the volume ratio of colloidal GO to H_2PtCl_6 in H_2O before diluted with ethanol. To test the stability and durability of the synthesized catalysts, they are prepared in the form of thin film on quartz substrate using a spray pyrolysis method. As the content of TRGO in the hybrid increases, the catalytic performance is considerably improved as shown in Fig. 4a-b. If the reduction reaction is assumed to follow first-order kinetics, the reaction rate constant is found to be as 0.012 min^{-1} for TRGO and 0.021 min^{-1} for pure Pt, and it increases to 0.036, 0.047, 0.066, and 0.080 min^{-1} for TRGO:Pt hybrids prepared with 1, 3, 5, and 7 mL of aqueous GO precursor, respectively. Figure 4c illustrates the stability and durability of the TRGO:Pt hybrid catalyst for the reduction of o-nitroaniline for eight cycles. Each cycle runs for 50 min. The catalytic efficiency is maintained at 90~97% for each cycle, which shows that the synthesized catalyst is highly stable and durable.

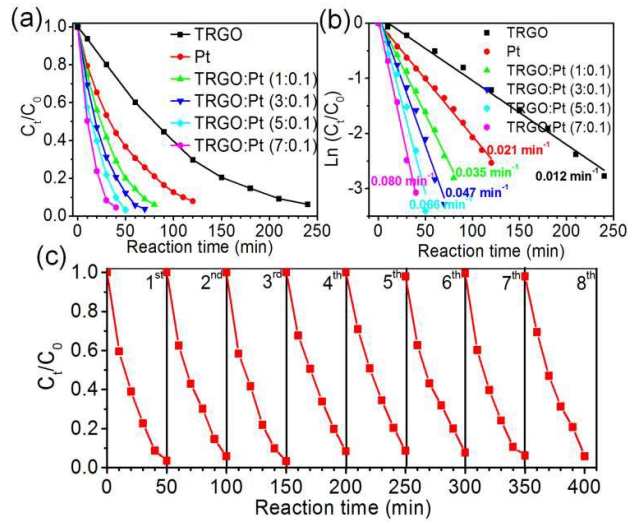

Figure 4. The catalytic performance of TRGO:Pt prepared at various amounts of colloidal GO (a). A plot of ln(Ct/C0) versus reaction time (b). The stability and durability of TRGO:Pt (5:0.1) for eight cycles (c).

Pt has been well-known as an excellent catalyst for hydrogenation reaction. In TRGO:Pt hybrids, Pt nanoparticles accept electrons from TRGO to enhance the ability of hydrogen chemisorption for catalytic reactivity. The reduction

mechanism of o-nitroaniline to 1,2-benzenediamine using a TGRO:Pt catalyst is described in Fig. 5. $NaBH_4$ reacts with water to generate hydrogen molecules which are attracted to the Pt surface by physisorption process and then are dissociated on the Pt surface by chemisorption process[34,35]. Hydrogen atoms produced reduce the $O=N^{+}\text{-}O^{-}$ group in o-nitroaniline to the NH_2 group as follows:

$NH_2(C_6H_4)NO_2 + 6H \rightarrow NH_2(C_6H_4)NH_2 + 2H_2O$

Due to a difference in work function between TRGO and Pt, electrons can transport from TRGO nanosheets to Pt nanoparticles[36,37], thus enhancing the electron perturbation at the Pt surface which easily dissociates hydrogen molecules chemisorbed on the Pt surface for catalytic reaction. Furthermore, an enhanced catalytic performance with an increase in TRGO amount in Fig. 4 indicates that TRGO works as the active site for catalytic reaction. The chemisorbed hydrogen atoms tend to spillover to TRGO network[38]. The negative surface of TRGO could attract the NO_2 terminal group of o-ntroaniline[34,39], reducing it to the NH_2 group. Thus, TRGO acts as a supporting material in improving the catalytic performance of Pt by providing electrons to the Pt surface and it also acts as an active site in catalytic reduction. The absorption spectra of o-nitroaniline reduced over TRGO:Pt catalysts with different composition are shown in Fig. S3 to monitor the reduction of o-nitroanilline to 1,2-benzendiamine. The absorption peaks appearing at 280 and 415 nm are indicative of the presence of o-nitroaniline. As the catalytic reduction proceeds, the intensity of the main peak at 415 nm is decreased and the peak at 280 nm is found to be red-shifted. A red-shifted of the peak from 280 to 290 nm with reaction time indicates that the reduction of o-nitroaniline to 1,2-benzenediamine has taken place[40].

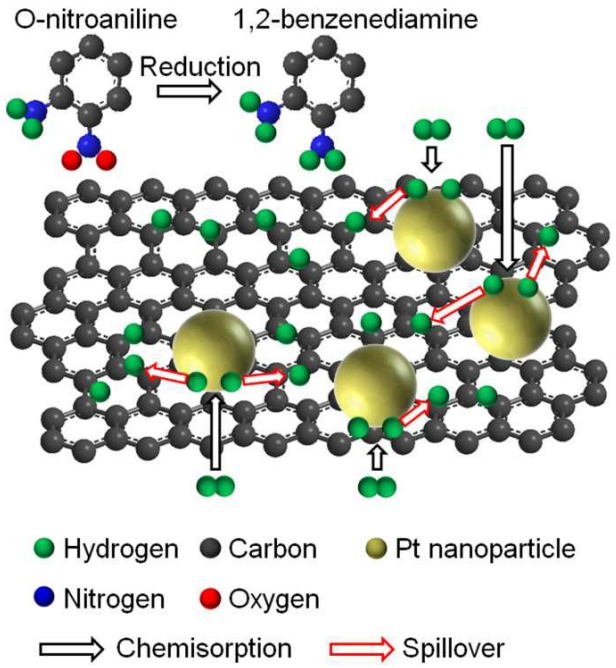

Figure 5. A schematic illustration of the reduction of o-nitroaniline to 1,2-benzenediamine over TRGO:Pt catalyst.

Taking advantage of its highly stable and effective catalytic activity, we fabricate DSSCs using TRGO:Pt as the counter electrode material. Figure 6a shows the cross-sectional SEM image of a TiO_2 photoanode which is prepared by applying TiO_2 paste to a FTO glass substrate using a doctor-blade technique. The thickness of the TiO_2 photoanode is 11 µm. The cross-sectional SEM images of a TRGO:Pt counter electrode with various TRGO/Pt ratios are shown in Fig. 6b-f. One can see that the TRGO:Pt is tightly adhered to the FTO glass substrate. The thickness of the TRGO:Pt slightly increases with an increase in the amount of colloidal GO precursor. The film thickness is 58 nm for Pt and increases to 67, 72, 81, and 86 nm for TRGO:Pt (1, 3, 5, and 7:0.1), respectively.

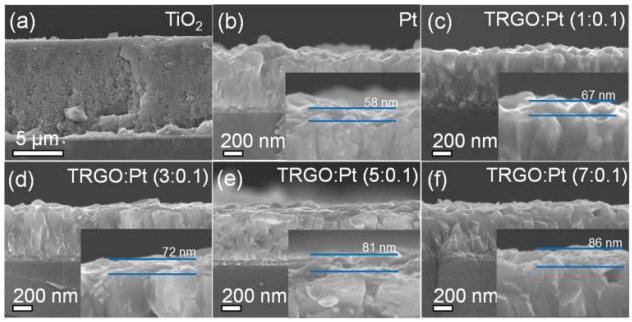

Figure 6. Cross-sectional FESEM images of TiO2 photoanode (a), Pt (b), and TRGO:Pt counter electrodes (c-f).

Figure 7 shows the cyclic voltammograms for the I^{-}/I_3^{-} redox reaction of different working electrodes. Positive current peaks are attributed to the oxidation reaction, while negative current peaks are ascribed to the reduction reaction[41,42]. The reduction peak at a lower voltage for TRGO:Pt has a higher current-response and is red-shifted by 0.1 V in comparison with Pt. This result implies that TRGO:Pt hybrid exhibits stronger and faster reduction reaction than Pt. Accordingly, the TRGO:Pt hybrid is an efficient counter electrode material for DSSCs to enhance the I^{-}/I_3^{-} electrolyte reduction process.

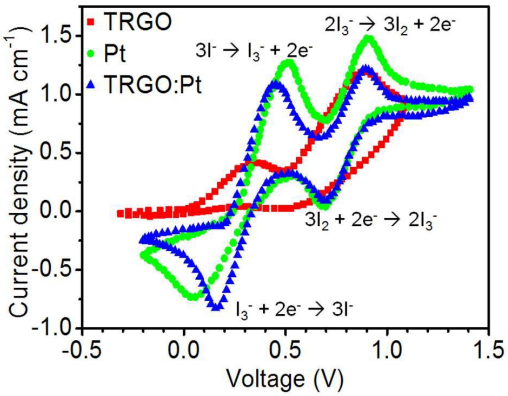

Figure 7. The cyclic voltammograms for the I^{-}/I_3^{-} redox reaction of different working electrodes including TRGO, Pt, and TRGO:Pt.

The electrochemical impedance spectra of DSSCs with different counter electrodes are shown in Fig. 8 to probe charge transfer at the interface between I^-/I_3^- electrolyte and counter electrode. The semicircle radius of TRGO:Pt hybrids is found to be smaller (indicating a lower charge transfer resistance) than that of Pt counter electrode. This result demonstrates that the TRGO:Pt is suitable for use as a counter electrode in DSSCs to increase a charge transfer rate at TRGO:Pt-I^-/I_3^- interface and reduce internal cell resistance.

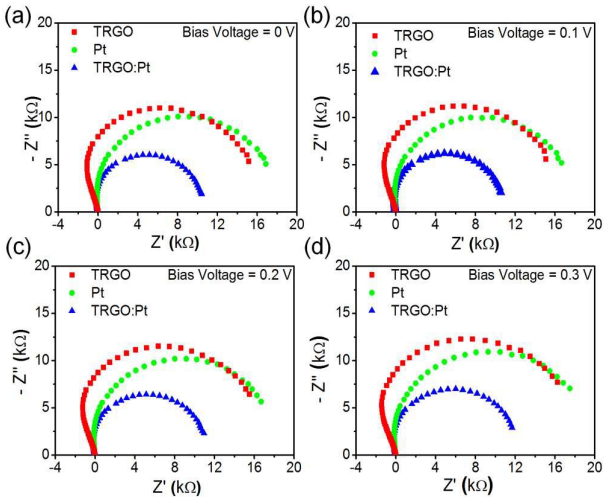

Figure 8. Nyquist plots of electrochemical impedance spectroscopy of TRGO, Pt, and TRGO:Pt at a bias voltage of 0 V (a), 0.1 V (b), 0.2 V (c), and 0.3 V (d).

Figure 9 shows the photovoltaic performance of DSSCs with different counter electrodes. The photoconversion efficiency (η) is 2.15% for the TRGO electrode and 4.31% for the Pt electrode. The η increases to 4.93, 5.19, 5.78, and 5.74% for the TRGO:Pt (1, 3, 5 and 7:0.1), respectively. It becomes saturated as 5.78% for the TRGO:Pt (5:0.1) electrode. The short circuit current density of DSSCs, Jsc, increases as the amount of colloidal GO precursor is increased. The TRGO:Pt (5:0.1) electrode is found to exhibit the best performance as shown in Fig. 9b and Table 1. TRGO:Pt hybrids are also evaluated for the catalytic reduction of I_3^- to I^- in the electrolyte of DSSCs to enhance photoconversion efficiency. As shown in Fig. 9, the short circuit current, Jsc, of the DSSCs increases with an increase in the amount of TRGO from 9.98 for pure Pt to 13.61 mA/cm^2 for TRGO:Pt hybrid (7:0.1). These results indicate that TRGO improves electron transport in the photoanode resulting in enhanced photovoltaic performance.

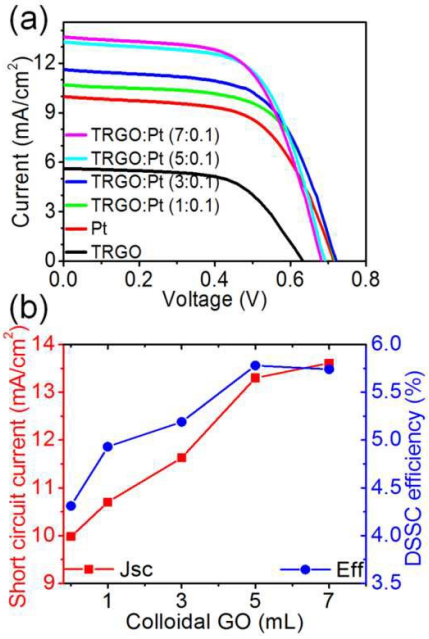

Figure 9. Photovoltaic performance of TiO2-based DSSCs using TRGO, Pt and TRGO:Pt counter electrodes (a), and the variation of short circuit current and DSSC efficiency with the amount of colloidal GO (b).

Table 1. Photovoltaic properties of TiO2-based DSSCs with a TRGO:Pt counter electrode.

Sample	Voc V	Jsc mA cm^{-2}	FF	Eff %
TRGO	0.64	5.61	0.60	2.15
Pt	0.71	9.98	0.61	4.31
TRGO:Pt (1:0.1)	0.72	10.70	0.64	4.93
TRGO:Pt (3:0.1)	0.72	11.63	0.62	5.19
TRGO:Pt (5:0.1)	0.69	13.30	0.63	5.78
TRGO:Pt (7:0.1)	0.68	13.61	0.62	5.74

Figure 10 schematically illustrates the role of TRGO in supplying electrons to reduce I_3^- thus increasing Jsc in a DSSC. Under solar irradiation, electrons are generated from dye and are diffused to the conduction band of TiO_2. At the same time, the dye is oxidized (D^+) and is then recovered by accepting an electron from I^- in the electrolyte[10,43]. I^- loses electrons to be I_3^-, and I_3^- receives electrons from the counter electrode to form I^- [10,11]. A number of D+ and I_3^- ions in the DSSC may recombine with electrons in dye and TiO_2, reducing the performance of the DSSC. When the Pt film is used as the counter electrode (Fig. 10a), electrons may not be supplied from Pt enough to reduce I_3^-, so the electron recombination would considerably occur. However, when the TRGO:Pt hybrid is used as the counter electrode (Fig. 10b), rapid electron transfer from TRGO to Pt at the interface and electron transfer from TRGO to the electrolyte greatly increase the reduction rate of I_3^-, thus reducing the recombination of photo-excited electrons in dye and TiO_2 photoanode, which enhances Jsc in the DSSC. Furthermore, the decoration of Pt nanoparticles on the TRGO surface increases the number of active sites for catalytic reduction of I_3^-.

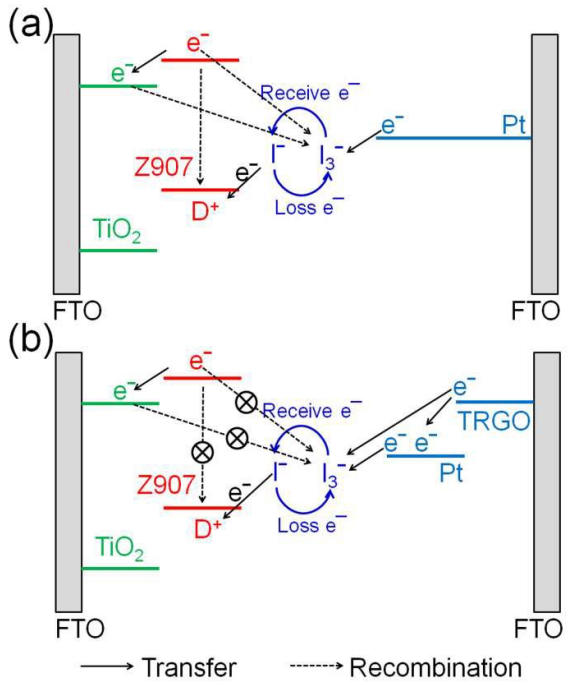

Figure 10. A schematic illustration of electron transfer in a DSSC using Pt (a) and TRGO:Pt (b) as the counter electrode.

Conclusions

We synthesize TRGO:Pt hybrids via a novel and facile solution method and evaluate them for use as a catalyst for the hydrogenation reaction of o-nitroaniline and a counter electrode in DSSCs. We demonstrate that TRGO with its negative network provides electrons to Pt and that it serves as a stabilizer for the uniform decoration of Pt nanopaticles on the Pt surface, which increases the number of catalytic active sites for the reduction of o-nitroaniline and I_3^-. The excellent catalytic performance of TRGO:Pt hybrids results in a significant increase in Jsc enhancing the efficiency of DSSCs.

Acknowledgements

This research was financially supported by Priority Research Centers Program (2009-0093818) and by the National Research Foundation of Korea (NRF-2014R1A4A1071686).

Notes and references

1 B. E. Hardin, H. J. Snaith and M. D. McGehee, *Nature Photonics,* 2012, **6,** 162.
2 B. O'Regan and M. Grätzel, *Nature,* 1991, **353,** 737.
3 N. A. Ludin, A. M. A. Mahmoud, A. B. Mohamad, A. A. H. Kadhum, K. Sopian and N. S. A. Karim, *Renew. Sustain. Energy Rev.,* 2014, **31,** 386.
4 A. Nattestad, A. J. Mozer, M. K. R. Fischer, Y. B. Cheng, A. Mishra, P. Bäuerle and U. Bach, *Nature Mater.,* 2010, **9,** 31.
5 J. Wu, Z. Lan, J. Lin, M. Huang, Y. Huang, L. Fan and G. Luo, *Chem. Rev.,* 2015, **115,** 2136.
6 M. Urbani, M. Grätzel, M. K. Nazeeruddin and T. Torres, *Chem. Rev.,* 2014, **114,** 12330.
7 Z. Chai, J. Gu, J. Khan, Y. Yuan, L. Du, X. Yu, M. Wu and W. Mai, *RSC Adv.,* 2015, **5,** 88052.
8 A. Akimov, A. J. Neukirch and O. V. Prezhdo, *Chem. Rev.,* 2013, **113,** 4496.
9 J. A. Anta, E. Guillén and R. Tena-Zaera, *J. Phys. Chem. C,* 2012, **116,** 11413.
10 A. Hagfeldt, G. Boschloo, L. Sun, L. Kloo and H. Pettersson, *Chem. Rev.,* 2010, **110,** 6595.
11 S. Thomas, T. G. Deepak, G. S. Anjusree, T. A. Arun, S. V. Nair and A. S. Nair, *J. Mater. Chem. A,* 2014, **2,** 4474.
12 H. Kim and J. S. Suh, *RSC Adv.,* 2015, **5,** 74107.
13 D. Bhattacharyya, P. K. Sarswat, M. Islam, G. Kumar, M. Misra and M. L. Free, RSC Adv., 2015, 5,70361.
14 Y. S. Kwon, I. Song, J. C. Lim, I. Y. Song, A. Siva and T. Park, *ACS Appl. Mater. Interfaces,* 2012, **4,** 3141.
15 T. Kinoshita, J. T. Dy, S. Uchida, T. Kubo and H. Segawa, *Nature Photonics,* 2013, **7,** 535.
16 G. Calogero, P. Calandra, A. Irrera, A. Sinopoli, I. Citro and G. D. Marco, *Energy Environ. Sci.,* 2011, **4,** 1838.
17 Z. Zheng, J. Chen, Y. Hu, W. Wu, J. Hua and H. Tian, *J. Mater. Chem. C,* 2014, **2,** 8497.
18 J. D. Roy-Mayhew, D. J. Bozym, C. Punckt and I. A. Aksay, *ASC Nano,* 2010, **4,** 6203.
19 W. J. Lee, E. Ramasamy, D. Y. Lee and J. S. Song, *ACS Appl. Mater. Interfaces,* 2009, **1,** 1145.
20 M. Chen, L. L. Shao, X. Qian, L. Liu, T. Z. Ren and Z. Y. Yuan, *Chem. Eng. J.,* 2014, **256,** 23.
21 M. H. Yeh, L. Y. Lin, C. L. Sun, Y. A. Leu, J. T. Tsai, C. Y. Yeh, R. Vittal and K. C. Ho, *J. Phys. Chem. C,* 2014, **118,** 16626.
22 G. Li, X. Chen and G. Gao, *Nanoscale,* 2014, **6,** 3283.
23 J. D. Roy-Mayhew and I. A. Aksay, *Chem. Rev.,* 2014, **114,** 6323.
24 Q. Luo, F. Hao, S. Wang, H. Shen, L. Zhao, J. Li, M. Gratzel and H. Lin, *J. Phys. Chem. C,* 2014, **118,** 17010.
25 S. P. Lim, A. Pandikumar, Y. S. Lim, N. M. Huang and H. N. Lim, *Scientific Reports,* 2014, **4,** 5305.
26 H. J. Ahn, I. H. Kim, J. C. Yoon, S. I. Kim and J. H. Jang, *Chem. Commun.,* 2014, **50,** 2412.
27 C. A. Lin, C. P. Lee, S. T. Ho, T. C. Wei, Y. W. Chi, K. P. Huang and J. H. He, *ACS Photonics,* 2014, **1,** 1264.
28 K. Saranya, N. Sivasankar and A. Subramania, *RSC Adv.,* 2014, **4,** 36226.
29 H. Bi, S. Sun, F. Huang, X. Xie and M. Jiang, *J. Mater. Chem.,* 2012, **22,** 411.
30 G. Wang, Y. Fang, Y. Lin, W. Xing and S. Zhuo, *Mater. Res. Bull.,* 2012, **47,** 4252.
31 Y. C. Hsu, G. L. Chen and R. H. Lee, *J. Polym. Res.,* 2014, **21,** 440.
32 K. C. Park, I. Y. Jang, W. Wongwiriyapan, S. Morimoto, Y. J. Kim, Y. C. Jung, T. Toya and M. Endo, *J. Mater. Chem.,* 2010, **20,** 5345.
33 S. Stankovich, R. D. Piner, X. Chen, N. Wu, S. T. Nguyen and R. S. Ruoff, *J. Mater. Chem.,* 2006, **16,** 155.
34 N. T. Khoa, S. W. Kim, D. H. Yoo, E. J. Kim and S. H Hahn, *Appl. Catal. A- Gen.,* 2014, **469,** 159.
35 J. Huang, L. Zhang, B. Chen, N. Ji, F. Chen, Y. Zhang and Z. Zhang, *Nanoscale,* 2010, **2,** 2733.
36 N. T. Khoa, S. W. Kim, D. H. Yoo, S. Cho, E. J. Kim and Hahn, *ACS Appl. Mater. Interfaces,* 2015, **7,** 3524.
37 G. Giovannetti, P. A. Khomyakov, G. Brocks, V. M. Karpan, J. van den Brink and P. J. Kelly, *Phys. Rev. Lett.,* 2008, **101,** 026803.
38 C. E. Hunt, *J. Catal.,* 1971, **23,** 93.
39 Y. Choi, H. S. Bae, E. Seo, S. Jang, K. H. Park and B. S. Kim, *J. Mater. Chem.,* 2011, **21,** 15431.

40 D. V. Thuan, N. T. Khoa, S. W. Kim, E. J. Kim and S. H. Hahn, *J. Catal.,* 2015, **329,** 144.
41 W. B. Dai, Y. F. Lei, P. Li and L. F. Xu, *J. Mater. Chem. A,* 2015, **3,** 4875.
42 S. Shukla, N. H. Loc, P. P. Boix, T. M. Koh, R. R. Prabhakar, H. K. Mulmudi, J. Zhang, S. Chen, C. F. Ng, C. H. A. Huan, N. Mathews, T. Sritharan and Q. Xiong, *ACS Nano,* 2014, **8,** 10597.
43 A. Nattestad, A. J. Mozer, K. M. R. Fischer, Y. B. Cheng, A. Mishra, P. Bäuerle and U. Bach, *Nature Mater.,* 2010, **9,** 31.

Graphical Abstract